Research article

Entesar Al-Hetlani*, Mohamed O. Amin and Metwally Madkour

Novel and versatile solid-state chemiluminescence sensor based on TiO_2-$Ru(bpy)_3^{2+}$ nanoparticles for pharmaceutical drugs detection

https://doi.org/10.1515/nanoph-2017-0104
Received October 24, 2017; revised November 26, 2017; accepted December 4, 2017

Abstract: This work describes a novel and versatile solid-state chemiluminescence sensor for analyte detection using TiO_2-$Ru(bpy)_3^{2+}$-Ce(IV). Herein, we report the synthesis, characterization, optimization and application of a new type of hybrid nanoparticles (NPs). Mesoporous TiO_2-$Ru(bpy)_3^{2+}$ NPs were prepared using a modified sol-gel method by incorporating $Ru(bpy)_3^{2+}$ into the initial reaction mixture at various concentrations. The resultant bright orange precipitate was characterized via transmission electron microscopy, N_2 sorpometry, inductively coupled plasma-optical emission spectrometer (ICP-OES), Raman and UV-Vis spectroscopy techniques. The concentration of $Ru(bpy)_3^{2+}$ complex in the NPs was quantified using ICP-OES, and its chemiluminescence (CL) response was measured and compared with the same concentration in the liquid phase using oxalate as model analyte. The results showed that this type of hybrid material exhibited a higher CL signal compared with the liquid phase due to the enlarged surface area of the hybrid NPs (~149.6 m^2/g). The amount of TiO_2-$Ru(bpy)_3^{2+}$ NPs and the effect of the analyte flow rate were also investigated to optimize the CL signal. The optimized system was further used to detect oxalate and two pharmaceutical drugs, namely, imipramine and promazine. The linear range for both drugs was 1–100 pM with limits of detection (LOD) of 0.1 and 0.5 pM, respectively. This approach is considered to be simple, low cost and facile and can be applied to a wide range of analytes.

Keywords: solid-state chemiluminescence; nanoparticles; detection; pharmaceutical drugs.

1 Introduction

Recently, many publications are concerned with the use of $Ru(bpy)_3^{2+}$ electrogenerated chemiluminescence (ECL) for the detection of several types of analytes [1, 2]. Intensive efforts have been devoted to $Ru(bpy)_3^{2+}$ solid-state ECL sensing platforms and their design over conventional chemiluminescence (CL). The reported strategies employed thus far mainly focused on utilizing solid supports in uniform dispersion or placing (positioning) them on the surface of the working electrode [3–6]. Examples of solid-state $Ru(bpy)_3^{2+}$ ECL sensors included the utilization of solid supports of various chemical natures, sizes and morphologies, to name a few: SiO_2 NPs [7], Sm_2O_3 NPs [8], graphene oxide [9] and carbon nanospheres [10]. In some cases, the solid support was used as a carrier for the $Ru(bpy)_3^{2+}$ molecules; in others, it played a dual role as a carrier and signal enhancer. Some of these solid supports are expensive to obtain and can be laborious to synthesize and functionalize. Generally, the CL reaction mechanism proposed for $Ru(bpy)_3^{2+}$ in the presence of a coreactant is as follows [11]:

$$Ru(bpy)_3^{2+} + \text{Oxidant (Ce(IV))} \rightarrow Ru(bpy)_3^{3+} + e^- \quad \text{Oxidation}$$

$$Ru(bpy)_3^{3+} + \text{Analyte} \rightarrow [Ru(bpy)_3^{2+}]^* \quad \text{Excitation}$$

$$[Ru(bpy)_3^{2+}]^* \rightarrow Ru(bpy)_3^{2+} + h\nu\,(610\ nm) \quad \text{Light emission}$$

Titania (TiO_2) NPs are semiconductors that have gained wide attention owing to their low cost of preparation, large yield and high surface area. Additionally, TiO_2 NPs are considered to be biologically and chemically inert and insoluble under most conditions, which extended their applications to areas such as in clinical and medical fields [12]. Moreover, they have been used in various applications such as photocatalysis [13], dye sensitization for

*Corresponding author: Entesar Al-Hetlani, Chemistry Department, Faculty of Science, Kuwait University, P.O. Box 5969, Safat 13060, Kuwait, e-mail: entesar.alhetlani@ku.edu.kw
Mohamed O. Amin and Metwally Madkour: Chemistry Department, Faculty of Science, Kuwait University, P.O. Box 5969, Safat 13060, Kuwait

Open Access. © 2018 Entesar Al-Hetlani et al., published by De Gruyter. BY-NC-ND This work is licensed under the Creative Commons Attribution-NonCommercial-NoDerivatives 4.0 License.

solar cells [14], degradation of pesticides [15] and hydrogen fuel production [16].

Previously, TiO_2 NPs have been used solely for solid-state ECL applications. A limited number of publications used such versatile material in $Ru(bpy)_3^{2+}$ ECL detection of various analytes in different types of samples. For example, $Ru(bpy)_3^{2+}$-TiO_2-perfluorosulfonated ionomer composite films were obtained through the immobilization of $Ru(bpy)_3^{2+}$ on TiO_2 NPs (size = 400 nm) in a multistep reaction by Choi et al. [17] in which sulfonation reaction on the surface of the TiO_2 NPs was carried out to form TiO_2-SO_3H. This was employed to enhance the electrostatic attraction between $Ru(bpy)_3^{2+}$ and the surface of the TiO_2 NPs for ECL applications. In this work, Nafion was employed to ensure the entrapment of the NPs on the electrode surface and their accessibility to the analytes in the solution. The tested analytes were tripropyl amine, oxalate and erythromycin in human urine samples. In another study conducted by Choi and coworkers [18], a more complex solid-state sensor was developed in a multistep preparation scheme, in which commercial multiwall carbon nanotubes (diameter, 10–20 nm; length, 10–50 mm) were solubilized in TiO_2 sol. This mixture was then introduced to an equal volume of Nafion polymer to stabilize the composite on the working electrode surface. The coated electrode was then dipped into a $Ru(bpy)_3^{2+}$ solution to immobilize it on the customized composite. The multiwall carbon nanotubes were incorporated to increase the amount of $Ru(bpy)_3^{2+}$ immobilized on the composite films and subsequently improve the CL signal for the detection of ethanol. Additionally, Xu and Yu [19] used TiO_2 nanotube (TN) arrays rather than NPs as a solid support to physically adsorb $Ru(bpy)_3^{2+}$ on their surface for amine detection in water sample. The immobilization of $Ru(bpy)_3^{2+}$ was performed by dipping the electrode in 0.1 M $Ru(bpy)_3^{2+}$ in phosphate buffer for 1 h at 65°C. The TNs were then coated with a drop of 0.1 M $Ru(bpy)_3^{2+}$ (volume was not specified) and dried three more times to ensure the immobilization of $Ru(bpy)_3^{2+}$ on the TNs. In this work, no polymer was used to stabilize the TiO_2 TNs on the surface of the electrode; the authors prepared their own electrode by growing the Ru-TNs on the surface of the Ti electrode.

To our knowledge, only two publications have dealt with the use of NPs for $Ru(bpy)_3^{2+}$ CL reactions, in which the NPs were used as coreactants to improve the CL signal owing to their oxidation/reduction properties and not as solid-state CL sensor [20, 21]. Although the idea of incorporating $Ru(bpy)_3^{2+}$ on a solid support for CL applications seem more simplistic and appealing, it has not yet been investigated. Additionally, no data for solid-state CL detection have been reported as opposed to the limited number of publications on solid-state ECL. Despite the fact that CL requires less demanding instrumentation compared with ECL: the use of expensive potentiostat, electrode fouling, polymers and electrolyte solutions are avoided. Additionally, incorporating $Ru(bpy)_3^{2+}$ complex into the TiO_2 NPs can be achieved in a single step rather than immobilizing it on the NP surface in a multistep and pH-controlled process, as previously been reported.

Thus, we report for the first time the synthesis and characterization of TiO_2-$Ru(bpy)_3^{2+}$ NPs by incorporating $Ru(bpy)_3^{2+}$ into TiO_2 sol in a one-pot reaction and their application as a solid-state CL sensor. This hybrid material was characterized to determine its size, morphology, porosity, surface area, $Ru(bpy)_3^{2+}$ concentration, UV-Vis absorption and Raman scattering spectra. Subsequently, the TiO_2-$Ru(bpy)_3^{2+}$ NPs were investigated for their CL activity for the detection of oxalate as a model analyte. The optimized system was then applied to two types of pharmaceutical drugs, imipramine and promazine, to show the versatility of the sensor.

2 Experimental

2.1 Reagents

Tris(2,2′-bipyridyl)dichlororuthenium(II) hexahydrate, ammonium cerium(IV) sulfate, sulfuric acid (95–97%), titanium tetrachloride ($TiCl_4$, 98%), ethanol (99.9%), sodium oxalate, promazine hydrochloride and imipramine hydrochloride were purchased from Sigma-Aldrich Chemie GmbH, Schnelldorf, Germany. Double-distilled water was used throughout all experiments. All chemicals were used as received without further purification.

2.2 Apparatus and equipment

The morphological properties of the TiO_2-$Ru(bpy)_3^{2+}$ NPs were determined using transmission electron microscopy (TEM) with a JEOL JEM 1230 (JEOL Ltd., Japan) operating at 120 kV. The optical properties of the samples were determined using UV-Vis spectra and were recorded using Agilent Cary 5000 UV-Vis spectrometer. Raman spectra of the NP samples were measured using Renishaw inVia confocal Raman spectrometer, with an excitation wavelength of 514 nm line of an argon ion laser and exposure time of 10 s and a grating of 2400 l/mm connected to a CCD camera detector. N_2 adsorption-desorption isotherms

were determined at –195°C using a model Gemini VII, ASAP 2020 automatic Micromeritics sorptometers (USA), equipped with an out gassing platform. Inductively coupled plasma-optical emission spectrometer (ICP-OES), Perkin Elmer, Optima 7300 DV, was used to measure the amounts of ruthenium and titanium in the TiO_2-$Ru(bpy)_3^{2+}$ NPs.

For CL detection, H11890-01 Photon Counting Head RoHS Conform (Hamamatsu Photonics UK Limited, Hertfordshire, UK) was used to collect the CL signal. The analyte was introduced into the reaction vial using a syringe pump (Graseby 3200, Worcs, UK).

2.3 Procedures

2.3.1 Preparation of TiO_2-$Ru(bpy)_3^{2+}$ NPs

The TiO_2 NPs were prepared as described in our previous work [13] with a minor modification. To the ethanol and water mixture, a certain amount of $Ru(bpy)_3^{2+}$ complex was added and allowed to dissolve at room temperature before adding the titanium precursor ($TiCl_4$). The amounts of $Ru(bpy)_3^{2+}$ were 0.692 and 0.069 g, which corresponded to 1:10 and 1:100 Ti:Ru molar ratio and referred to in the text as diluted and concentrated, respectively. The formed NPs were washed repeatedly with ethanol and dried overnight under vacuum at 50°C.

2.3.2 Sample preparation for ICP-OES

A 0.1 g of TiO_2-$Ru(bpy)_3^{2+}$ NPs was digested using block digestion in acidic solution (mixture of HNO_3:HCl:H_2O_2). The digestate was subsequently analyzed using ICP-OES.

2.3.3 CL of TiO_2-$Ru(bpy)_3^{2+}$ NPs

The setup consisted of a homemade wooden box in which the photon counting head was placed and isolated from external light source. The CL reaction was performed in a glass vial that contained a certain amount of TiO_2-$Ru(bpy)_3^{2+}$ NPs, which was then mixed with 1 ml of 5 mM ammonium cerium(IV) sulfate in 0.25 M sulfuric acid solution and placed directly on top of the photon counting head using a homemade plastic holder. The oxidant was added to the TiO_2-$Ru(bpy)_3^{2+}$ NPs using a micropipette and vortexed to form a green dispersion. The analyte was introduced to the mix using a syringe pump to control the addition flow rate as illustrated in Figure 1.

3 Results and discussion

3.1 Characterization of TiO_2-$Ru(bpy)_3^{2+}$ NPs

3.1.1 Size and morphology

The surface morphology of plain TiO_2, diluted and concentrated TiO_2-$Ru(bpy)_3^{2+}$ NPs was determined by TEM (Figure 2A–C). TEM images of the synthesized TiO_2 NPs showed small size particles (~5 nm) of irregular semi-spherical shape, which remained almost unchanged in the hybrid TiO_2-$Ru(bpy)_3^{2+}$ NPs. The $Ru(bpy)_3^{2+}$ complex was shown to be homogeneously dispersed on TiO_2 NPs.

3.1.2 N_2 isotherms

The N_2 isotherms and their pore size vs. pore volume data were obtained for all three samples: plain TiO_2 and diluted

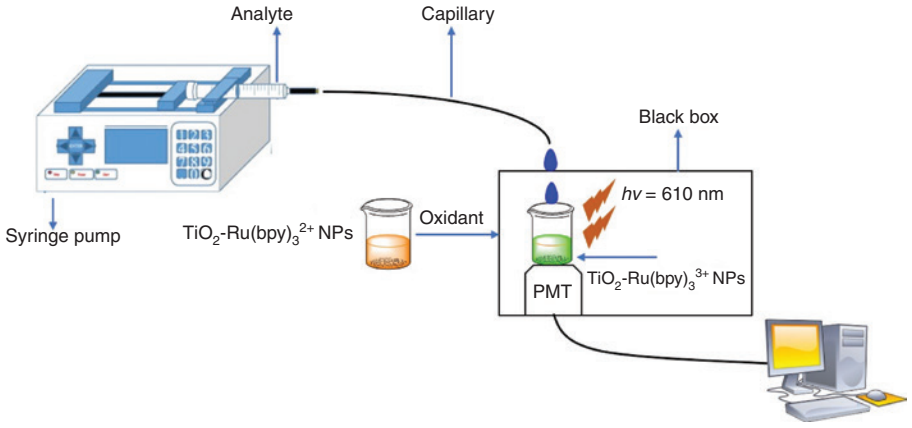

Figure 1: A schematic representation of the experiemental setup and reaction scheme for the TiO_2-$Ru(bpy)_3^{2+}$ solid-state CL sensor.

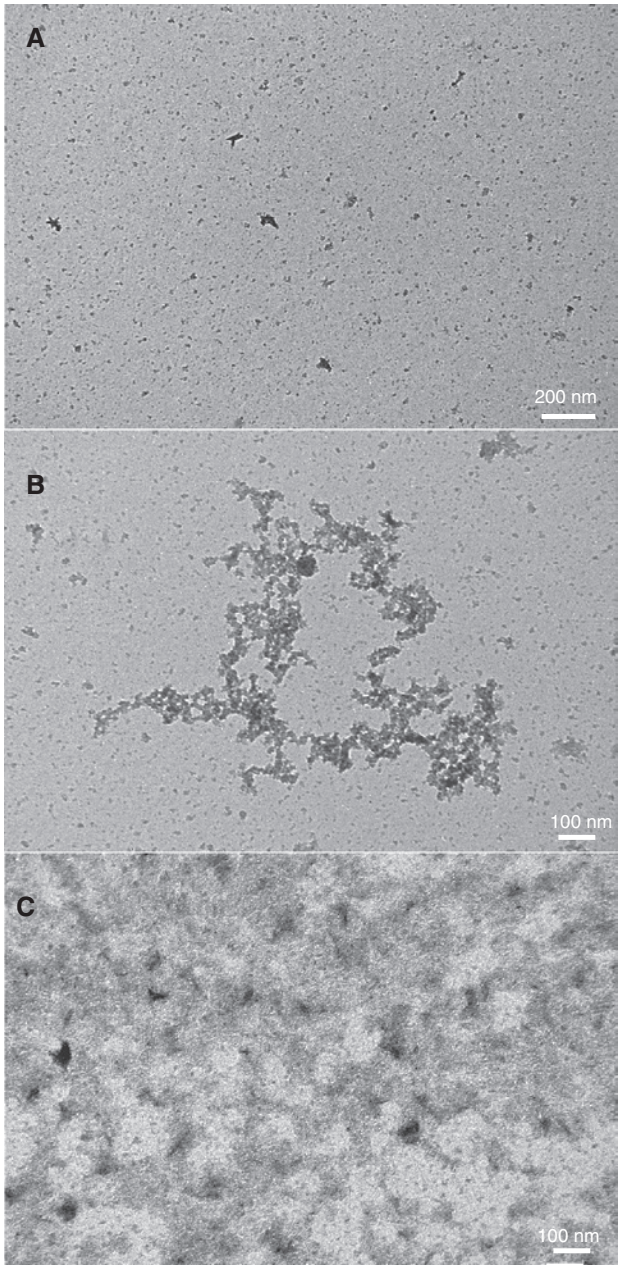

Figure 2: TEM images of the (A) plain TiO_2 and (B) diluted and (C) concentrated TiO_2-$Ru(bpy)_3^{2+}$ NPs.

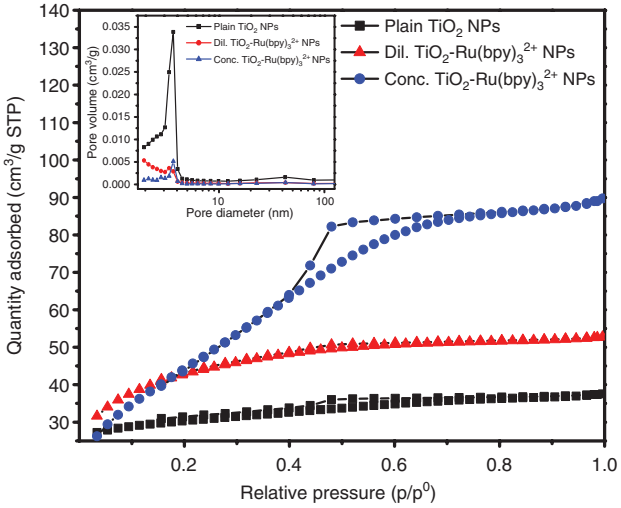

Figure 3: N_2 adsorption-desorption isotherms of the plain TiO_2, diluted and concentrated TiO_2-$Ru(bpy)_3^{2+}$ NPs.
The inset is the pore size distributions for the samples.

Table 1: Barrett-Joyner-Halenda average pore diameter (D_p), volume (V_p) and specific surface area (S_{BET}) for the plain TiO_2 and diluted and concentrated TiO_2-$Ru(bpy)_3^{2+}$ NPs.

Sample	Pore diameter (nm)	Pore volume (cm^3/g)	Surface area (m^2/g)
TiO_2 NPs	3.12	0.15	197.8
Diluted TiO_2-$Ru(bpy)_3^{2+}$ NPs	2.18	0.081	149.6
Concentrated TiO_2-$Ru(bpy)_3^{2+}$ NPs	2.94	0.027	36.9

and concentrated TiO_2-$Ru(bpy)_3^{2+}$ NPs (Figure 3), while the pore size, pore volume and surface area for the same samples are displayed in Table 1. N_2 isotherms obtained for all samples can be ascribed as type IV, and the hysteresis loop can be classified in the middle between H2 and H4 types, indicating a mesoporous structure with slit-shaped pores.

Furthermore, N_2 sorpometry measurements shown in Table 1 revealed that the incorporation and the concentration of $Ru(bpy)_3^{2+}$ with the TiO_2 NP surface had a detrimental effect on the specific surface area. It was observed that as the amount of $Ru(bpy)_3^{2+}$ increased, the surface area and pore volume of the hybrid NPs decreased. This could be attributed to the amount of TiO_2 present in both the diluted and concentrated TiO_2-$Ru(bpy)_3^{2+}$ NPs, which is less compared with the pure TiO_2 NPs (also supported by the ICP data, discussed later). As the TiO_2 NPs only contributed to the surface area and porosity of the TiO_2-$Ru(bpy)_3^{2+}$ NPs, lowering the amount of TiO_2 in the NPs caused the reduction in the surface area and pore volume.

3.1.3 UV-Vis spectroscopy

The absorption spectra of the plain TiO_2, diluted TiO_2-$Ru(bpy)_3^{2+}$ and concentrated TiO_2-$Ru(bpy)_3^{2+}$ NPs were measured using UV-Vis spectrometer in the range of 200–800 nm, as shown in Figure 4A.

UV-Vis spectrum of the plain TiO_2 NPs exhibited a sharp peak at 360 nm owing to the transitions of electrons

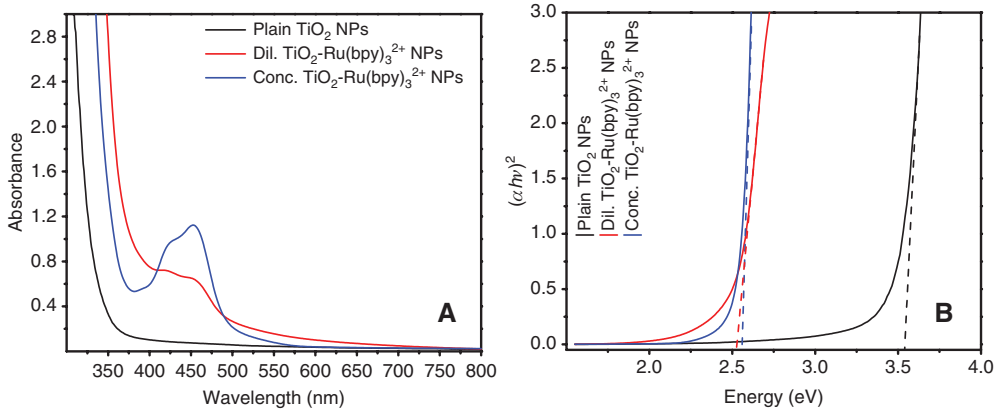

Figure 4: (A) UV-Vis absorption spectra of the plain TiO_2, diluted TiO_2-$Ru(bpy)_3^{2+}$ and concentrated TiO_2-$Ru(bpy)_3^{2+}$ NPs. (B) A plot of $(\alpha h\nu)^2$ vs. $h\nu$ for the plain TiO_2, diluted TiO_2-$Ru(bpy)_3^{2+}$ and concentrated TiO_2-$Ru(bpy)_3^{2+}$ NPs.

from valence band to conductance band. However, the UV-Vis spectra of the diluted and concentrated TiO_2-$Ru(bpy)_3^{2+}$ NPs showed two absorption peaks: the characteristic absorption band of TiO_2 NPs at 360 nm, in addition to the band at 450 nm, which is ascribed to the $Ru(bpy)_3^{2+}$ complex metal-to-ligand charge transfer (MLCT) [22]. This indicated the successful incorporation of $Ru(bpy)_3^{2+}$ complex in the TiO_2 NPs and formation of the hybrid material.

Additionally, almost no difference in $\lambda_{max} = 450$ nm between the TiO_2-$Ru(bpy)_3^{2+}$ NPs and liquid phase $Ru(bpy)_3^{2+}$ (data not shown) can be observed, which is an indication of the negligible surface association between $Ru(bpy)_3^{2+}$ molecules and TiO_2 NPs [23]. Quantitatively, the peak at 450 nm for diluted and concentrated TiO_2-$Ru(bpy)_3^{2+}$ NPs showed a difference in peak intensity, which can be related to the $Ru(bpy)_3^{2+}$ concentration (or loading capacity) in the TiO_2-$Ru(bpy)_3^{2+}$ NPs. A higher intensity was observed with the concentrated TiO_2-$Ru(bpy)_3^{2+}$ NPs compared with the diluted ones.

From the UV-Vis spectra, a red shift was observed for the TiO_2 NPs in the presence of the $Ru(bpy)_3^{2+}$. The band gap values of the plain TiO_2, diluted TiO_2-$Ru(bpy)_3^{2+}$ and concentrated TiO_2-$Ru(bpy)_3^{2+}$ NPs were calculated according to Tauc method using the following equation:

$$(\alpha h\nu)1/m = k(h\nu - E_g)$$

where E_g is the optical band gap energy, k is a constant and $m = 1/2$ for a direct energy band gap. For this purpose, a plot of $(\alpha h\nu)^2$ vs. $h\nu$ was constructed, and the linear portion of the plot was extrapolated to the ordinate as shown in Figure 4B. The values were 3.53, 2.53 and 2.57 eV for TiO_2, diluted TiO_2-$Ru(bpy)_3^{2+}$ and concentrated TiO_2-$Ru(bpy)_3^{2+}$ NPs, respectively.

3.1.4 Raman spectroscopy

Figure 5 shows the Raman spectra obtained for the plain TiO_2, diluted and concentrated TiO_2-$Ru(bpy)_3^{2+}$ NPs. The Raman spectrum of the plain TiO_2 NPs was dominated by four active modes detected at 150, 402, 512 and 636 cm^{-1}, which can be assigned to the vibrational modes of the pure anatase phase of TiO_2 NPs [24].

On the other hand, the Raman spectrum of the diluted TiO_2-$Ru(bpy)_3^{2+}$ NPs showed additional peaks at 1021, 1168 and 1353 cm^{-1}, which can be attributed to the presence of $Ru(bpy)_3^{2+}$ in the TiO_2 NPs [25]. Furthermore, a stronger enhancement of 1050, 1180, 1285 and 1353 cm^{-1} vibration bands and a decrease in band intensity for 150, 402, 512 and 636 cm^{-1} were observed for the concentrated TiO_2-$Ru(bpy)_3^{2+}$ NPs, owing to the presence of larger amounts of $Ru(bpy)_3^{2+}$ in the TiO_2 NPs.

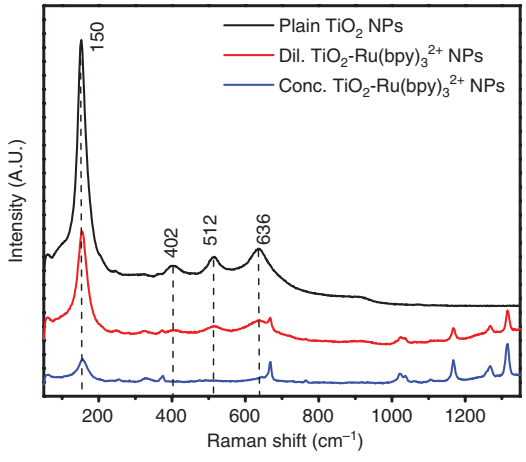

Figure 5: Raman spectra of the plain TiO_2, diluted TiO_2-$Ru(bpy)_3^{2+}$ and concentrated TiO_2-$Ru(bpy)_3^{2+}$ NPs.

3.1.5 ICP-OES

For the diluted and concentrated TiO_2-$Ru(bpy)_3^{2+}$ NPs, the amount of $Ru(bpy)_3^{2+}$ incorporated into TiO_2 NPs was determined by using ICP-OES. For the diluted TiO_2-$Ru(bpy)_3^{2+}$ NPs (1:100 Ti:Ru molar ratio), the molar concentrations of Ti and Ru metals in the TiO_2-$Ru(bpy)_3^{2+}$ NPs were 3.75×10^{-3} and 3.42×10^{-5} M, respectively. Whereas for the concentrated TiO_2-$Ru(bpy)_3^{2+}$ NPs (1:10 Ti:Ru molar ratio), the values were 1.8×10^{-3} and 3×10^{-4} M, respectively. This was an indication of incorporation of the $Ru(bpy)_3^{2+}$ into the TiO_2 NPs. Moreover, as the loaded amount of Ru in TiO_2 NPs increased, the concentration of Ru in TiO_2 hybrid is also increased.

3.2 Testing the solid-state CL TiO_2-$Ru(bpy)_3^{2+}$ NP sensor using oxalate

3.2.1 Control experiment

As a proof of concept, CL was investigated for the plain TiO_2 NPs and the diluted (3×10^{-4} M) and concentrated (3.42×10^{-5} M) solutions of $Ru(bpy)_3^{2+}$ in 0.25 M sulfuric acid. In addition, the synthesized diluted and concentrated hybrid TiO_2-$Ru(bpy)_3^{2+}$ NPs were also tested. Oxalate was used as a model analyte owing to its low cost and intense CL response (Figure 6).

The results showed that the plain TiO_2 NPs did not exhibit any CL signal after adding the Ce(IV) and oxalate. On the other hand, in the presence of $Ru(bpy)_3^{2+}$ solution, the signal was affected by the concentration of $Ru(bpy)_3^{2+}$. The higher concentration of $Ru(bpy)_3^{2+}$ produced a lower CL signal compared with the lower concentration of $Ru(bpy)_3^{2+}$, which could be attributed to the low concentration of the oxidant used. In the case of both diluted and concentrated TiO_2-$Ru(bpy)_3^{2+}$ NPs, the CL signals were comparable, and the diluted concentration was slightly higher than the concentrated one, which was consistent with the liquid phase results.

Interestingly, the TiO_2-$Ru(bpy)_3^{2+}$ NPs produced signals higher than the aqueous system, which was due to the large surface area of TiO_2-$Ru(bpy)_3^{2+}$ NPs, providing better interaction between the $Ru(bpy)_3^{2+}$ and both the oxidant and oxalate.

For further experiments, the diluted TiO_2-$Ru(bpy)_3^{2+}$ NPs were utilized because they contained smaller amounts of $Ru(bpy)_3^{2+}$.

3.2.2 Effect of the flow rate

To explore the optimum experimental conditions of the constructed solid-state CL sensor, the flow rate at which the analyte was introduced into the TiO_2-$Ru(bpy)_3^{3+}$ NPs was investigated. The CL signal was measured at flow rates of 100, 125, 150, 175 and 200 ml/h, and the results are shown in Figure 7.

As can be seen from the figure, as the flow rate increased, the CL signal also increased, which is consistent with previously reported data [26]. The maximum CL signal was obtained using a 200-ml/h flow rate. Unfortunately, because of the flow rate restriction from the syringe pump, higher flow rates could not be explored.

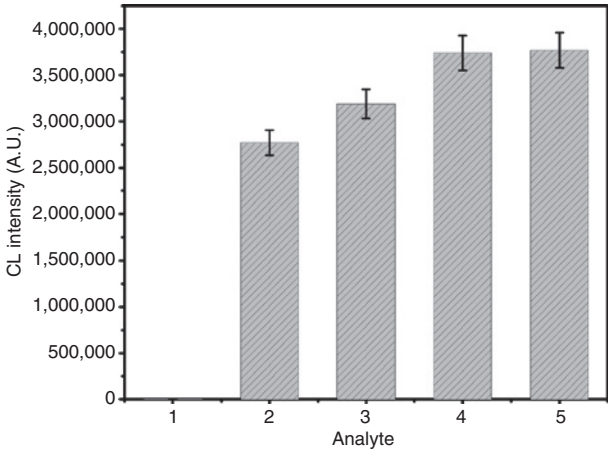

Figure 6: The CL signal detected using 0.5 mM Ce(IV) in 0.25 M sulfuric acid as oxidant and 1 mM oxalate as the analyte: 1, plain TiO_2 NPs; 2, concentrated $Ru(bpy)_3^{2+}$ aqueous solution; 3, diluted $Ru(bpy)_3^{2+}$ aqueous solution; 4, concentrated TiO_2-$Ru(bpy)_3^{2+}$ NPs; 5, diluted TiO_2-$Ru(bpy)_3^{2+}$ NPs.

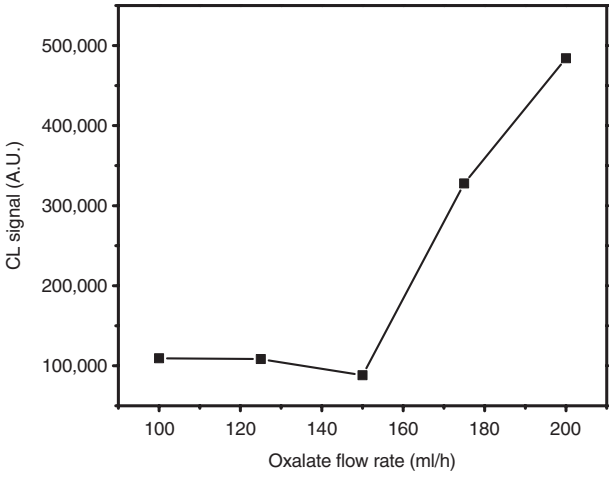

Figure 7: The effect of analyte (oxalate) flow rate (ml/h) on CL signal using diluted TiO_2-$Ru(bpy)_3^{3+}$ NPs.

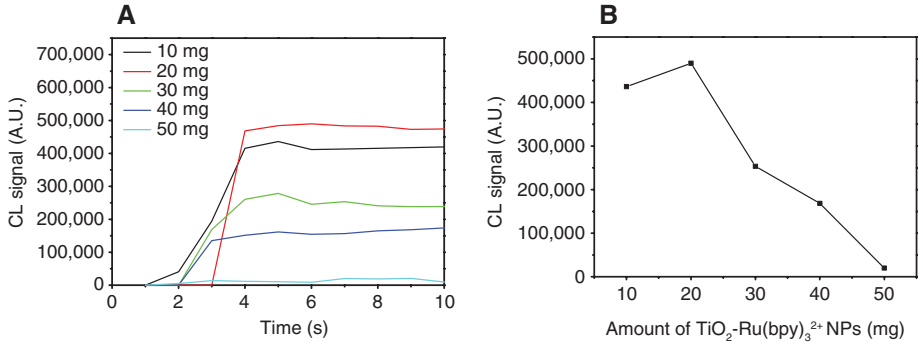

Figure 8: (A) The individual CL signal vs. time using different amounts of TiO_2-$Ru(bpy)_3^{2+}$ NPs. (B) The effect of the amount of TiO_2-$Ru(bpy)_3^{2+}$ NPs (mg) using oxalate as an analyte at a flow rate of 200 ml/h.

For the rest of the experiments, analyte flow rate addition of 200 ml/h was used.

3.2.3 Effect of the amount of TiO_2-$Ru(bpy)_3^{2+}$ NPs

Considering the amount of TiO_2-$Ru(bpy)_3^{2+}$ NPs on the CL signal is a vital parameter; thus, the effect of the amount (in mg) used in each experiment was studied. Quantities of 10, 20, 30, 40 and 50 mg of the TiO_2-$Ru(bpy)_3^{2+}$ NPs were tested using 0.5 mM Ce(IV) and oxalate solution (Figure 8A and B). Thus, the optimum amount of the TiO_2-$Ru(bpy)_3^{2+}$ NPs was 20 mg, which is considered suitable as higher amounts are undesirable for low-cost and efficient systems.

3.2.4 Calibration using oxalate

Oxalate detection is very useful in areas of food chemistry [27] and clinical analysis [28, 29]. For example, monitoring the amount of oxalate in blood or urine can help physicians diagnose certain illnesses such as kidney diseases [30]. One way to monitor the concentration of oxalate is using conventional $Ru(bpy)_3^{2+}$ CL or ECL [31, 32]. Thus, we used oxalate as one of the analytes to test the TiO_2-$Ru(bpy)_3^{2+}$ NP CL system; the reaction mechanism can be found elsewhere [33]. Besides the optimization reported above, a calibration curve was constructed for oxalate as shown in Figure 9.

The linear range obtained for oxalate was between 10 and 100 pM using our TiO_2-$Ru(bpy)_3^{2+}$ NP CL sensor as illustrated in Figure 9, with LOD of 1 pM. The values of the linear detection range and LOD for oxalate reported in the literature using different types of CL/ECL systems are shown in Table 2. Compared with the tabulated results, the TiO_2-$Ru(bpy)_3^{2+}$ NP solid-state sensor has improved

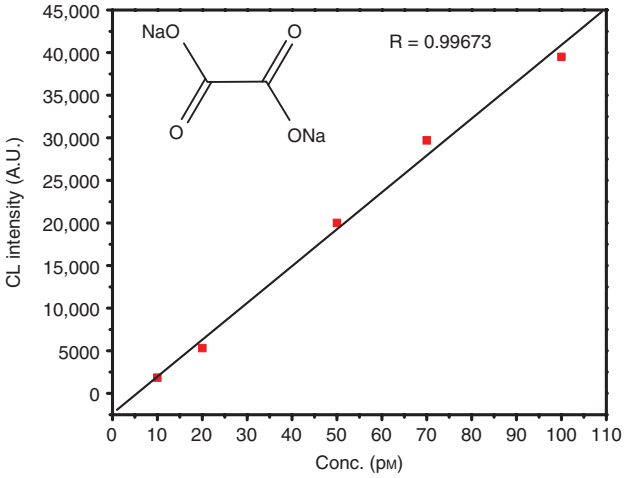

Figure 9: Calibration curve obtained for sodium oxalate using diluted TiO_2-$Ru(bpy)_3^{2+}$ NPs.
Conditions: 0.5 mM Ce(IV) and 200 ml/h flow rate. The oxalate structure is also shown.

the linear range and lowered the LOD of oxalate compared with that of previous work that reported using CL and ECL.

3.2.5 Testing the solid-state CL sensor using pharmaceutical drugs

The TiO_2-$Ru(bpy)_3^{2+}$ NP sensor was further exploited to detect two pharmaceutical drugs, namely, imipramine and promazine. Imipramine is an example of tricyclic antidepressant drugs, which are commonly prescribed for the treatment of depression and other psychiatric disorders [39], whereas promazine is used as an antipsychotic and an antiemetic agent [40]. A calibration curve for both imipramine and promazine was plotted using the optimized conditions as shown in Figure 10A and B.

Table 2: Linear range and LOD of oxalate determined using different types of CL sensors found in the literature.

CL sensor type	Linear range	LOD	Reference
TiO_2-SO_3-$Ru(bpy)_3^{2+}$ solid-state ECL	1 μM–1 mM	1.0 μM	Choi et al. [17]
Flow injection instrumentation	ND	5 μM	Barnett et al. [27]
Aqueous ECL	ND	ND	Rubinstein and Bard [34]
Aqueous solution ECL	10^{-6}–10^{-4} M	ND	Rubinstein et al. [35]
Aqueous CL	1.4×10^{-5}–1.4×10^{-7} M	2.7×10^{-8} M	He and Gao [36]
HPLC-CL	1×10^{-5}–4×10^{-3} M	6.2×10^{-6} M	Wu et al. [37]
Three types: (1) external generation, (2) *in situ* generation and (3) immobilized $Ru(bpy)_3^{2+}$ in Nafion	0.5–10,000 μM	0.5 μM	Lee and Nieman [38]
Solid-state TiO_2-$Ru(bpy)_3^{2+}$ NP CL	10–100 pM	1 pM	This work

ND, Not determined.

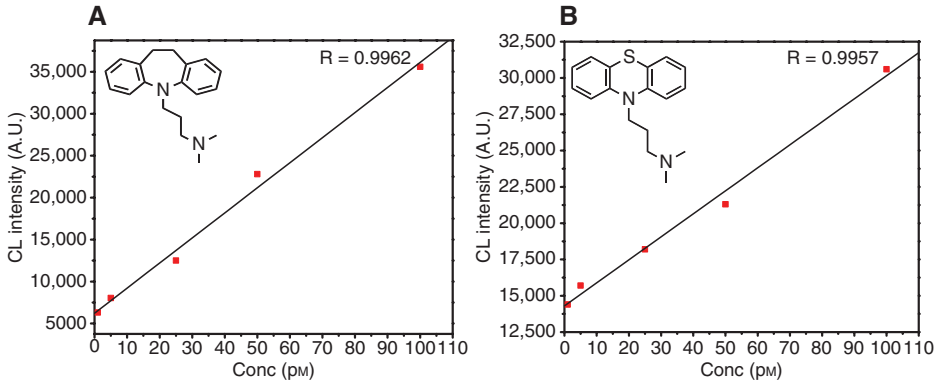

Figure 10: Calibration curve for (A) imipramine drug and (B) promazine drug.
Conditions: 0.5 mM Ce(IV) and 200 ml/h flow rate. The structures of the drugs are also shown.

The linear range obtained for imipramine was 1–100 pM using TiO_2-$Ru(bpy)_3^{2+}$ NPs. Compared with a recently published data by Sedaghati and coworkers [41], which relied on a quite complicated ECL system, rather than CL, based on $Ru(bpy)_3^{2+}$-palladium NPs doped carbon ionic liquid electrode, they reported linearity and LOD similar to our TiO_2-$Ru(bpy)_3^{2+}$ NPs sensor. Additionally, promazine showed a linear range similar to that obtained for imipramine with LOD of 0.5 pM. Previously reported data for promazine involved the use of $Ru(bpy)_3^{2+}$-Ce(IV) in acidic media. The reported linear range was 0.4–30.0 μg/ml and LOD of 0.1 μg/ml [42].

4 Conclusion

A simple, rapid and low-cost detection system based on solid-state CL as opposed to ECL was lucratively developed. The TiO_2-$Ru(bpy)_3^{2+}$ NPs was prepared, characterized and used for CL detection of oxalate, imipramine and promazine. The detection system operated well for the detection of the analytes without the need for polymers for temporal and spatial control or expensive electrical components to help generate and detect the CL signal. The developed system was optimized and can be applied to various types of analytes with improved LOD than previously reported data in the literature. This system could be transferred to a microfluidic platform for better efficiencies and applied to real life samples using minute amounts of reagents and analytes.

Acknowledgments: The authors gratefully acknowledge the support of the Kuwait University Research Administration for funding project numbers SC 02/17 and SC 06/16. Special thanks to RSPU Facilities (GS 01/01, GS 02/01, GS 03/01 and NUERS (srul 01/13)).

References

[1] Nepomnyashchii AB, Kolesov G, Parkinson BA. Electrogenerated chemiluminescence of BODIPY, $Ru(bpy)_3^{2+}$, and 9,10-diphenylanthracene using interdigitated array electrodes. ACS Appl Mater Interfaces 2013;5:5931–6.

[2] Ma H, Li X, Yan T, et al. Sensitive insulin detection based on electrogenerated chemiluminescence resonance energy transfer between $Ru(bpy)_3^{2+}$ and Au nanoparticle-doped-cyclodextrin-Pb (II) metal organic framework. ACS Appl Mater Interfaces 2016;8:10121–7.
[3] Zhuang Y, Ju H. Determination of reduced nicotinamide adenine dinucleotide based on immobilization of tris(2,2′-bipyridyl) ruthenium(II) in multiwall carbon nanotubes/Nafion composite membrane. Anal Lett 2005;38:2077–88.
[4] Sun X, Du Y, Dong S, Wang E. Method for effective immobilization of $Ru(bpy)_3^{2+}$ on an electrode surface for solid-state electrochemiluminescene detection. Anal Chem 2005;77:8166–9.
[5] Qian L, Yang XR. One-step synthesis of $Ru(2,2'\text{-bipyridine})_3Cl_2$-immobilized silica nanoparticles for use in electrogenerated chemiluminescence detection. Adv Funct Mater 2007;17:1353–8.
[6] Bertoncello P, Stewart AJ, Dennany L. Analytical applications of nanomaterials in electrogenerated chemiluminescence. Anal Bioanal Chem 2014;406:5573–87.
[7] Spehar-Délèze A-M, Almadaghi S, Sullivan C. Development of solid-state electrochemiluminescence (ECL) sensor based on Ru(bpy)32+-encapsulated silica nanoparticles for the detection of biogenic polyamines. Chemosensors 2015;3:178–89.
[8] Hosseini M, Moghaddam MR, Faridbod F, Norouzi P, Pur MRK, Ganjali MR. A novel solid-state electrochemiluminescence sensor based on a Ru(bpy)32+/nano Sm_2O_3 modified carbon paste electrode for the determination of l-proline. RSC Adv 2015;5:64669–74.
[9] Pur MRK, Hosseini M, Faridbod F, Dezfuli AS, Ganjali MR. A novel solid-state electrochemiluminescence sensor for detection of cytochrome c based on ceria nanoparticles decorated with reduced graphene oxide nanocomposite. Anal Bioanal Chem 2016;408:7193–202.
[10] Zhang A, Miao C, Shi H, Xiang H, Huang C, Jia N. A novel solid-state electrochemiluminescence sensor for atropine determination based on Ru(bpy)32+/carbon nanospheres/Nafion composite film. Sens Actuators B 2016;222:433–9.
[11] Gerardi RD, Barnett NW, Lewis AW. Analytical applications of tris(2,2′-bipyridyl)ruthenium(III) as a chemiluminescent reagent. Anal Chim Acta 1999;378:1–41.
[12] Bumajdad A, Madkour M. Understanding the superior photocatalytic activity of noble metals modified titania under UV and visible light irradiation. Phys Chem Chem Phys 2014;16: 7146–58.
[13] Al-Hetlani E, Amin MO, Madkour M. Detachable photocatalysts of anatase TiO_2 nanoparticles: annulling surface charge for immediate photocatalyst separation. Appl Surf Sci 2017;411:355–62.
[14] Sivaram V, Crossland EJW, Leijtens T, et al. Observation of annealing-induced doping in TiO_2 mesoporous single crystals for use in solid state sye sensitized solar cells. J Phys Chem C 2014;118:1821–7.
[15] Barakat NAM, Nassar MM, Farrag TE, Mahmoud MS. Effective photodegradation of methomyl pesticide in concentrated solutions by novel enhancement of the photocatalytic activity of TiO_2 using $CdSO_4$ nanoparticles. Environ Sci Pollut Res 2014;21:1425–35.
[16] Wu B, Liu D, Mubeen S, Chuong TT, Moskovits M, Stucky GD. Anisotropic growth of TiO_2 onto gold nanorods for plasmon-enhanced hydrogen production from water reduction. J Am Chem Soc 2016;138:1114–7.
[17] Choi HN, Cho S-H, Lee W-Y. Electrogenerated chemiluminescence from tris(2,2′-bipyridyl)ruthenium(II) immobilized in titania perfluorosulfonated ionomer composite films. Anal Chem 2003;75:4250–6.
[18] Choi HN, Yoon SH, Lyu Y-K, Lee W-Y. Electrogenerated chemiluminescence ethanol biosensor based on carbon nanotube-titania-Nafion composite film. Electroanalysis 2007;19:459–65.
[19] Xu Z, Yu J. A novel solid-state electrochemiluminescence sensor based on $Ru(bpy)_3^{2+}$ immobilization on TiO_2 nanotube arrays and its application for detection of amines in water. Nanotechnology 2010;21:245501.
[20] Amjadi M, Hallaj T. Dramatic enhancement effect of carbon quantum dots on the chemiluminescence of –Ce(IV) reaction and application to the determination of 4-nitrophenol. J Lumin 2016;171:202–7.
[21] Gorman BA, Francis PS, Dunstan DE, Barnett NW. Tris(2,2′-bipyridyl)ruthenium(II) chemiluminescence enhanced by silver nanoparticles. Chem Commun 2007;395–7.
[22] Innocenzi P, Kozuka H, Yoko T. Fluorescence properties of the $Ru(bpy)_3^{2+}$ complex incorporated in sol-gel-derived silica coating films. J Phys Chem B 1997;101:2285–91.
[23] Zang L, Rodgers MAJ. Diffusion-controlled charge transfer from excited $Ru(bpy)_3^{2+}$ into nanosized TiO_2 colloids stabilized with EDTA. J Phys Chem B 2000;104:468–74.
[24] Chen X, Lou YB, Samia ACS, Burda C, Gole JL. Formation of oxynitride as the photocatalytic enhancing site in nitrogen-doped titania nanocatalysts: comparison to a commercial nanopowder. Adv Funct Mater 2005;15:41–9.
[25] Silverstein DW, Milojevich CB, Camden JP, Jensen L. Investigation of linear and nonlinear Raman scattering for isotopologues of $Ru(bpy)_3^{2+}$. J Phys Chem C 2013;117:20855–66.
[26] Barnett W, Bowser TA, Gerardi RD, Smith B. Determination of codeine in process streams using flow-injection analysis with chemiluminescence detection. Anal Chim Acta 1996;318:309–17.
[27] Barnett NW, Lewis SW, Purcell SD, Jones P. Determination of sodium oxalate in Bayer liquor using flow-analysis incorporating an anion exchange column and tris(2,2′-bipyridyl) ruthenium(II) chemiluminescence detection. Anal Chim Acta 2002;458:291–6.
[28] Holmes RP, Kennedy M. Estimation of the oxalate content of foods and daily oxalate intake. Kidney Int 2000;57:1662–7.
[29] Cao LC, Jonassen J, Honeyman TW, Scheid C. Oxalate-induced redistribution of phosphatidylserine in renal epithelial cells. Am J Nephrol 2001;21:69–77.
[30] Ermer T, Eckardt K-U, Aronson PS, Knauf F. Oxalate, inflammasome, and progression of kidney disease. Curr Opin Nephrol Hypertens 2016;25:363–71.
[31] Lee W-Y, Nieman TA. Effect of organic solvent on tris(2,2′-bipyridyl)ruthenium(III) chemiluminescent reactions in flowing streams. Anal Chim Acta 1996;334:183–91.
[32] Skotty R, Lee W-Y, Nieman TA. Determination of dansyl amino acids and oxalate by HPLC with electrogenerated chemiluminescence detection using tris(2,2′-bipyridyl)ruthenium(II) in the mobile phase. Anal Chem 1996;68:1530–5.
[33] Chiu M-H, Wu H, Chen J-C, Muthuraman G, Zen J-M. Disposable screen-printed carbon electrodes for dual electrochemiluminescence/amperometric detection: sequential injection analysis of oxalate. Electroanalysis 2007;19:2301–6.

[34] Rubinstein I, Bard AJ. Electrogenerated chemiluminescence. 37. Aqueous ecl systems based on tris(2,2′-bipyridine) ruthenium(2+) and oxalate or organic acids. J Am Chem Soc 1981;103:512–6.
[35] Rubinstein I, Martin CR, Bard AJ. Electrogenerated chemiluminescent determination of oxalate. Anal Chem 1983;55:1580–2.
[36] He Z, Gao H. Simultaneous determination of oxalic and tartaric acid with chemiluminescence detection. Analyst 1997;122:1343–6.
[37] Wu F, He Z, Luo Q, Zeng YE. HPLC determination of oxalic acid using tris(1,10-phenanthroline)ruthenium(II) chemiluminescence–application to the analysis of spinach. Food Chem 1999;65:543–6.
[38] Lee W-Y, Nieman TA. Evaluation of use of tris(2,2′-bipyridyl) ruthenium(III) as a chemiluminescent reagent for quantitation in flowing streams. Anal Chem 1995;67:1789–96.
[39] de Toledo RA, Santos MC, Honório KM, da Silva ABF, Cavalheiro ETG, Mazo LH. Use of graphite polyurethane composite electrode for imipramine oxidation–mechanism proposal and electroanalytical determination. Anal Lett 2006;39:507–20.
[40] Lara FJ, García-Campaña AM, Alés-Barrero F, Bosque-Sendra JM. Determination of thiazinamium, promazine and promethazine in pharmaceutical formulations using a CZE method. Anal Chim Acta 2005;535:101–8.
[41] Safavi A, Banazadeh A, Sedaghati F. Synthesis of palladium nanoparticles on organically modified silica: application to design of a solid-state electrochemiluminescence sensor for highly sensitive determination of imipramine. Anal Chim Acta 2013;796:115–21.
[42] Ensafi AA, Hasanpour F, Khayamian T. Simultaneous chemiluminescence determination of promazine and fluphenazine using support vector regression. Talanta 2009;79:534–8.